

# Stracherite, $\text{BaCa}_6(\text{SiO}_4)_2[(\text{PO}_4)(\text{CO}_3)]\text{F}$ , the first $\text{CO}_3$ -bearing intercalated hexagonal antiperovskite from Negev Desert, Israel

EVGENY V. GALUSKIN<sup>1,\*</sup>, BILJANA KRÜGER<sup>2</sup>, IRINA O. GALUSKINA<sup>1</sup>, HANNES KRÜGER<sup>2</sup>,  
YEYGENY VAPNIK<sup>3</sup>, ANUSCHKA PAULUHN<sup>4</sup>, AND VINCENT OLIERIC<sup>4</sup>

<sup>1</sup>Faculty of Earth Sciences, Department of Geochemistry, Mineralogy and Petrography, University of Silesia, Będzińska 60, 41-200 Sosnowiec, Poland

<sup>2</sup>Institute of Mineralogy and Petrography, University of Innsbruck, Innrain 52, 6020, Innsbruck, Austria

<sup>3</sup>Department of Geological and Environmental Sciences, Ben-Gurion University of the Negev, POB 653, Beer-Sheva 84105, Israel

<sup>4</sup>Swiss Light Source, Paul Scherrer Institute, 5232 Villigen, Switzerland

## ABSTRACT

The new mineral stracherite,  $\text{BaCa}_6(\text{SiO}_4)_2[(\text{PO}_4)(\text{CO}_3)]\text{F}$  [ $R\bar{3}m$ ,  $a = 7.0877(5) \text{ \AA}$ ,  $c = 25.201(2) \text{ \AA}$ ,  $V = 1096.4(1) \text{ \AA}^3$ ,  $Z = 3$ ], belongs to the zadovite group, which also includes zadovite,  $\text{BaCa}_6[(\text{SiO}_4)(\text{PO}_4)](\text{PO}_4)_2\text{F}$ ; aradite,  $\text{BaCa}_6[(\text{SiO}_4)(\text{VO}_4)](\text{VO}_4)_2\text{F}$ ; and gazeevite,  $\text{BaCa}_6(\text{SiO}_4)_2(\text{SO}_4)_2\text{O}$ . All minerals of this group exhibit single-layer antiperovskite modules, which are intercalated with tetrahedral layers. In stracherite, the first  $\text{CO}_3$ -bearing intercalated hexagonal antiperovskite, about 38% of the  $(\text{PO}_4)^{3-}$  tetrahedra are randomly substituted by planar  $(\text{CO}_3)^{2-}$  groups. The mineral was discovered in spurrite rocks of the Hatrurim Complex in the Negev Desert near Arad, Israel. Associated minerals are spurrite, calcite, brownmillerite, shulamitite,  $\text{CO}_3$ -bearing fluorapatite, fluormayenite-fluorkyuygenite, and ariegilatite. The empirical formula of stracherite is:  $(\text{Ba}_{0.96}\text{K}_{0.02}\text{Na}_{0.01})_{\Sigma 0.99}\text{Ca}_{6.01}[(\text{SiO}_4)_{1.86}(\text{PO}_4)_{0.12}(\text{AlO}_4)_{0.01}(\text{TiO}_4)_{0.01}]_{\Sigma 2}[(\text{PO}_4)_{1.05}(\text{CO}_3)_{0.75}(\text{SO}_4)_{0.18}(\text{VO}_4)_{0.02}]_{\Sigma 2}(\text{F}_{0.95}\text{O}_{0.03})_{\Sigma 0.98}$ . Poikilitic crystals of stracherite are up to 0.5 mm in size and are confined to re-crystallization zones of spurrite marbles under the influence of by-products (gases, fluids) of combustion metamorphism.

**Keywords:** Stracherite, zadovite group, new mineral, intercalated hexagonal antiperovskites,  $\text{CO}_3$ , Raman, pyrometamorphic rocks, Hatrurim Complex

## INTRODUCTION

Stracherite,  $\text{BaCa}_6(\text{SiO}_4)_2[(\text{PO}_4)(\text{CO}_3)]\text{F}$  [ $R\bar{3}m$ ,  $a = 7.0877(5)$ ,  $c = 25.201(2) \text{ \AA}$ ,  $V = 1096.4(1) \text{ \AA}^3$ ,  $Z = 3$ ], was discovered in spurrite rocks of the Hatrurim Complex in the Negev Desert near Arad, Israel. It is the fourth mineral isotypic with zadovite (see Table 1 in Galuskin et al. 2018). Minerals with zadovite-type structure can be considered as intercalated hexagonal antiperovskites with a general formula of  $AB_6(\text{TO}_4)_2(\text{TO}_4)_2W$ , where  $A = \text{Ba, K, ...}$ ;  $B = \text{Ca, Na}$ ;  $T = \text{Si, P, V}^{5+}, \text{S}^{6+}, \text{Al, ...}$ ;  $W = \text{O}^{2-}, \text{F}^-$ , and antiperovskite layers  $[(W_6B_6)(\text{TO}_4)_2]^{6+}$  and  $A(\text{TO}_4)_2$  layers occur in a ratio of 1:1. There are three zadovite-group minerals: zadovite,  $\text{BaCa}_6[(\text{SiO}_4)(\text{PO}_4)](\text{PO}_4)_2\text{F}$ ; aradite  $\text{BaCa}_6[(\text{SiO}_4)(\text{VO}_4)](\text{VO}_4)_2\text{F}$ ; and gazeevite,  $\text{BaCa}_6(\text{SiO}_4)_2(\text{SO}_4)_2\text{O}$  (Galuskin et al. 2015a, 2017). Stracherite is the first mineral of this group to exhibit a substitution of  $(\text{PO}_4)^{3-}$  tetrahedra by planar  $(\text{CO}_3)^{2-}$  groups. Consequently, tetrahedral modules  $\text{Ba}[(\text{PO}_4)(\text{CO}_2)]^{3-}$  alternate with  $[\text{FCa}_6(\text{SiO}_4)_2]^{3+}$  antiperovskite modules.

Minerals of the nabimusaite group can also be considered as intercalated hexagonal antiperovskites but with a general formula of the form  $AB_{12}(\text{TO}_4)_4(\text{TO}_4)_2W_3$  ( $A, B, T$ , and  $W$  are as indicated above). However, in this structure type, single tetrahedral layers  $A(\text{TO}_4)_2$  are intercalated with triple antiperovskite layers  $[(W_3B_{12})(\text{TO}_4)_4]^{6+}$  resulting in a 3:1 ratio of the structural modules. The mineral nabimusaite,  $\text{KCa}_{12}(\text{SiO}_4)_4(\text{SO}_4)_2\text{O}_2\text{F}$  [ $R\bar{3}m$ ,  $a = 7.1905(4)$ ,  $c = 41.251(3) \text{ \AA}$ ,  $V = 1847.1(2) \text{ \AA}^3$ ,  $Z = 3$ ],

was the first intercalated hexagonal antiperovskite detected in pyrometamorphic rocks of the Hatrurim Complex (Galuskin et al. 2015b). Nabimusaite is an isotype of arctite,  $\text{Ba}(\text{Ca}_7\text{Na}_9)(\text{PO}_4)_4(\text{PO}_4)_2\text{F}_3$  ( $R\bar{3}m$ ,  $a = 7.094 \text{ \AA}$ ,  $c = 41.320 \text{ \AA}$ ; Sokolova et al. 1984). Later, dargaite,  $\text{BaCa}_{12}(\text{SiO}_4)_4(\text{SO}_4)_2\text{O}_3$ , and ariegilatite,  $\text{BaCa}_{12}(\text{SiO}_4)_4(\text{PO}_4)_2\text{OF}_2$ , were found and confirmed to be members of the nabimusaite group (Krüger et al. 2017; Galuskin et al. 2018; Galuskin et al. 2018). Triple antiperovskite layers in minerals of this group resemble triple antiperovskite layers in the structure of hatrurite-framework hexagonal antiperovskite (Jeffery 1952; Krivovichev 2008; Galuskin et al. 2015b).

The name stracherite is given in honor of the well-known American geologist, Glenn Blair Stracher (aka “The Firewalker,” born March 31, 1949, in Albany, New York), Professor Emeritus of Geology at East Georgia State College in Swainsboro, Georgia, U.S.A. Stracher is the author and editor of numerous scientific works on coal combustion and chemical thermodynamics. He also authored books, including the GSA Engineering Geology Book and the five volumes of Coal and Peat Fire Elsevier books. Stracher edited and supported the publication of our earliest works related to the study of the Hatrurim Complex in Israel (Vapnik et al. 2007). He is the co-author of our recent study related to the fascinating discovery of stone tool workshops utilizing pyrometamorphic rocks of the Hatrurim Basin (Vapnik et al. 2015).

The mineral and name (IMA2016-098) were approved by the Commission on New Minerals, Nomenclature and Classification (CNMNC) of the International Mineralogical Association (IMA).

\* E-mail: evgeny.galuskin@us.edu.pl

Type material was deposited in the mineralogical collection of the Fersman Mineralogical Museum, Moscow, Russia; catalog numbers: 4957/1.

### METHODS OF INVESTIGATION

Crystal morphology and chemical composition of stracherite and associated minerals were examined using an optical microscope, as well as a Philips XL30 and a Phenom XL analytical electron scanning microscopes (Faculty of Earth Sciences, University of Silesia, Poland). Chemical analyses of stracherite were performed with a CAMECA SX100 microprobe (Institute of Geochemistry, Mineralogy and Petrology, University of Warsaw, Poland) at 15 kV and 10 nA using the following lines and standards: BaL $\alpha$ , SK $\alpha$  = baryte; PK $\alpha$  = fluorapatite; CaK $\alpha$  = wollastonite; SiK $\alpha$  = diopside; VK $\alpha$  = V<sub>2</sub>O<sub>5</sub>; AlK $\alpha$ , KK $\alpha$  = orthoclase; TiK $\alpha$  = rutile; NaK $\alpha$  = albite; SrL $\alpha$  = SrTiO<sub>3</sub>; FK $\alpha$  = fluorphlogopite.

The Raman spectrum of stracherite was recorded on a WITec  $\alpha$  300R confocal Raman microscope (Department of Earth Science, University of Silesia, Poland) equipped with an air-cooled solid laser 532 nm and a CCD camera operating at -61 °C. The laser radiation was coupled to a microscope through a single-mode optical fiber with a diameter of 3.5  $\mu$ m. An air Zeiss LD EC Epiplan-Neofluan DIC-100/0.75NA objective was used. Raman scattered light was focused on a broad band single mode fiber with an effective pinhole size of 30  $\mu$ m. A monochromator with a 600 mm<sup>-1</sup> grating was used. The power of the laser at the sample position was ca. 40 mW. Integration intervals of 10 s with an accumulation of 15 scans and a resolution of 3 cm<sup>-1</sup> were chosen. The monochromator was calibrated using the Raman scattering line of a silicon plate (520.7 cm<sup>-1</sup>).

Diffraction experiments were performed using a single crystal of stracherite (~87 × 50 × 30  $\mu$ m) at the Beamline X06DA, Swiss Light Source, Paul Scherrer Institute, Villigen, Switzerland (Waltersperger et al. 2015). Data were processed (including absorption correction) using the XDS software package (Kabsch 2010). The atomic coordinates of zadovite (Galuskin et al. 2015a) were used as a starting model. With subsequent analyses of difference-Fourier maps, the position of (CO<sub>3</sub>)<sup>2-</sup> groups was located and the crystal structure was refined to R1 = 2.19%. The refinements include anisotropic atom displacement parameters and have been carried out with neutral atom scattering factors, using the program SHELX97 (Sheldrick 2008).

### ORIGIN AND DESCRIPTION OF STRACHERITE

Stracherite, BaCa<sub>6</sub>(SiO<sub>4</sub>)<sub>2</sub>[(PO<sub>4</sub>)(CO<sub>3</sub>)<sub>2</sub>F], was found in spurrite pyrometamorphic rocks of the Hatrurim Complex in the Negev Desert (N31°13'58" E35°16'2") near Arad, Israel. Associated minerals are spurrite, calcite, brownmillerite, shulamitite, CO<sub>3</sub>-bearing fluorapatite, fluormayenite-fluorkyuygenite, periclase, brucite, barytocalcite, baryte, garnets of elbrusite-kerimasite series, undiagnosed Ca-Fe and Rb-bearing K-Fe sulfides, the new mineral ariegilatite (Krüger et al. 2017a; Galuskin et al. 2018) and a potentially new mineral Ba<sub>2</sub>Ca<sub>18</sub>(SiO<sub>4</sub>)<sub>6</sub>(PO<sub>4</sub>)<sub>3</sub>(CO<sub>3</sub>)F<sub>3</sub>O (Krüger et al. 2017b).

Stracherite is confined to altered spurrite rocks with an abundance of small calcite veins. It was also observed in concentric formations, which we interpret as gaseous channels (microfumaroles) filled with fine-grained calcite-spurrite aggregates and plenty of Ca- and K-Fe-sulfides (Fig. 1, zone I). Channel walls of this microfumaroles are formed by large spurrite poikilitic crystals (metacrysts) up to 1 cm in length (Fig. 1, zone II). For comparison, in unaltered spurrite marbles, spurrite grains usually do not exceed the size of 100  $\mu$ m. Nevertheless, rare and relatively large metacrysts of stracherite, up to 0.5 mm in size, are found at the boundary of zone I and II (Figs. 1, 2, and 3a). Also, smaller grains of stracherite, less than 100  $\mu$ m, occur in the fine-grained part of spurrite rock (zone III, Fig. 1).

Stracherite crystals are flattened on {001} and often exhibit a hexagonal shape in cross sections perpendicular to *c* (Figs. 2a–2c and 3a). Stracherite substitutes for CO<sub>3</sub>-bearing

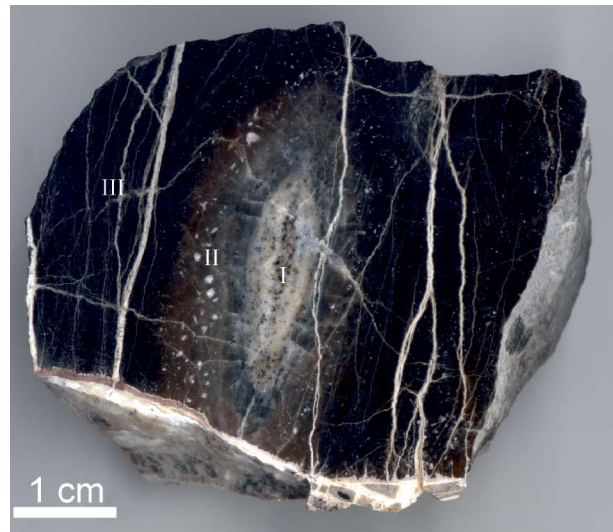


**FIGURE 1.** Rare example of a gaseous channel (microfumarole) filled with a fine-grained spurrite and calcite with accessory shulamitite and unidentified Ca- and K-Fe-sulfides (zone I), with large spurrite metacrysts, up to 1 cm in size, forming the walls of the channel (zone II). Zone III is represented by fine-grained spurrite rock with an abundance of brownmillerite. Large stracherite metacrysts have grown in a gray intermediate area between zones I and II.

fluorapatite (Fig. 3b). Occasionally, oriented overgrowths of stracherite on ariegilatite can be observed as well as substitutions of stracherite for ariegilatite (Fig. 3c). An induction surface of cooperative growth of stracherite with large spurrite metacrysts was recorded (Fig. 2d).

Stracherite is a colorless mineral with glassy luster and a white streak. It does not fluoresce. This mineral is optically uniaxial, positive:  $\omega = 1.635(2)$ ,  $\epsilon = 1.659(2)$  ( $\lambda = 589$  nm). The measured microhardness VHN<sub>50</sub> = 510(12) kg/mm<sup>2</sup> (average of 15 measurements), range between 490 and 540 kg/mm<sup>2</sup>. Hence, Mohs hardness is about 5. Cleavage is imperfect on (001), and parting is not observed. Stracherite is brittle with irregular fractures. The abundance of tiny inclusions of spurrite, fluormayenite, calcite, brownmillerite, etc., does not allow to select pure grains for density measurement. Consequently, the calculated density is 3.365 g/cm<sup>3</sup>. Gladstone-Dale's compatibility factor [ $1 - (K_p/K_c)$ ] was calculated to -0.026 (excellent), using the appropriate empirical formula (Mandarino 2007). Stracherite is homogeneous and its empirical formula is (Table 1, average of 22 measurements): (Ba<sub>0.96</sub>K<sub>0.02</sub>Na<sub>0.01</sub>)<sub>20.99</sub>Ca<sub>6.01</sub>[(SiO<sub>4</sub>)<sub>1.86</sub>(PO<sub>4</sub>)<sub>0.12</sub>(AlO<sub>4</sub>)<sub>0.01</sub>(TiO<sub>4</sub>)<sub>0.01</sub>]<sub>22</sub>[(PO<sub>4</sub>)<sub>1.05</sub>(CO<sub>3</sub>)<sub>0.75</sub>(SO<sub>4</sub>)<sub>0.18</sub>(VO<sub>4</sub>)<sub>0.02</sub>]<sub>22</sub>(F<sub>0.95</sub>O<sub>0.03</sub>)<sub>20.98</sub>. About 38% of the (PO<sub>4</sub>)<sup>3-</sup> tetrahedra in stracherite are substituted by planar (CO<sub>3</sub>)<sup>2-</sup> groups. This was confirmed by structural refinement and Raman spectroscopy investigations (see below). Sulfur, which enters tetrahedral sites as (SO<sub>4</sub>)<sup>2-</sup> anion groups, is a significant impurity (SO<sub>3</sub> ~ 2 wt%).

### Raman spectroscopy

Unpolarized Raman spectra of stracherite and CO<sub>3</sub>-bearing fluorapatite were obtained from the same grain, which was used to determine the chemical composition (Table 1). The experimental spectra with the results of peak fitting in the region 80–1500 cm<sup>-1</sup>

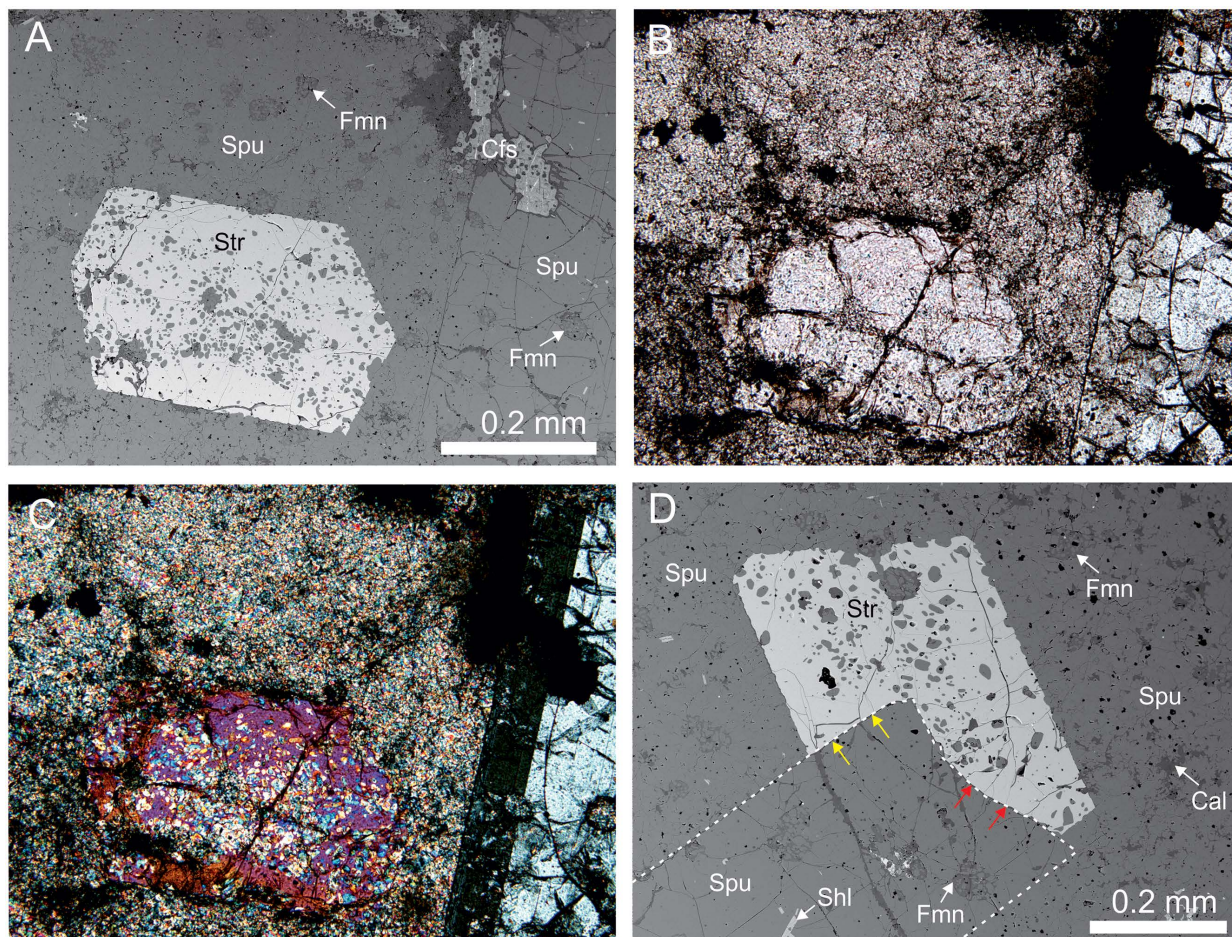


**FIGURE 2.** (a–c) One of the biggest stracherite metacrysts, its fragments were used for structural and optical investigations: (a) BSE image; (b and c) transmitted light: (b) parallel nicols, (c) crossed nicols; (d) intergrowth of stracherite and spurrite indicating their simultaneous growth. Yellow arrows show idiomorphic surface, and red arrows = induction surface of cooperative growth of stracherite and spurrite. Str = stracherite, Spu = spurrite, Shu = shulamitite, Fmn = fluormayenite-fluorkyuygenite, Cal = calcite, Cfs = undiagnosed Ca-Fe sulfide.

are presented in Figure 4. The main bands of stracherite are related to vibrations of  $(\text{CO}_3)^{2-}$ ,  $(\text{PO}_4)^{3-}$ , and  $(\text{SiO}_4)^{4-}$  groups analogous to  $\text{CO}_3$ -bearing apatite and hydroxyllestadite (Penel et al. 1998; Comodi and Liu 2000; Banno et al. 2016). The main bands in the spectrum of stracherite are (Fig. 4a,  $\text{cm}^{-1}$ ):  $1408 \nu_3(\text{CO}_3)^{2-}$ ;  $1069 \nu_1(\text{CO}_3)^{2-}$ ;  $1036 \nu_3(\text{PO}_4)^{3-}$ ;  $995 \nu_1(\text{SO}_4)^{2-}$ ;  $952 \nu_1(\text{PO}_4)^{3-}$ ;  $858 \nu_1(\text{SiO}_4)^{4-}$ ;  $704 \nu_4(\text{CO}_3)^{2-}$ ;  $623 \nu_4(\text{SO}_4)^{2-}$ ;  $584$  and  $555 \nu_4(\text{PO}_4)^{3-}$ ;  $518 \nu_4(\text{SiO}_4)^{4-}$ ;  $431 \nu_2(\text{PO}_4)^{3-}$ ;  $399 \nu_2(\text{SiO}_4)^{4-}$ ;  $335$ ,  $307$ ,  $225$ ,  $210$ ,  $114$  (lattice modes, Ca-O, Ba-O vibrations). The main bands in the spectrum of  $\text{CO}_3$ -bearing apatite, which is substituted by stracherite, are also connected with vibrations of  $(\text{PO}_4)^{3-}$ ,  $(\text{CO}_3)^{2-}$ , and  $(\text{SiO}_4)^{4-}$  ( $\text{cm}^{-1}$ , Fig. 4b):  $1072 \nu_1(\text{CO}_3)^{2-}$ ;  $962 \nu_1(\text{PO}_4)^{3-}$ ;  $859 \nu_1(\text{SiO}_4)^{4-}$ ;  $586 \nu_4(\text{PO}_4)^{3-}$ ;  $428 \nu_2(\text{PO}_4)^{3-}$ . The band caused by stretching vibration of the  $(\text{CO}_3)^{2-}$  group is located nearly at the same Raman shift in stracherite and  $\text{CO}_3$ -bearing apatite (Fig. 4):  $1069$  and  $1072 \text{ cm}^{-1}$ , respectively. In the spectrum of stracherite containing  $\sim 4.4 \text{ wt}\%$   $\text{CO}_2$  a band from bending vibrations of the  $\text{CO}_3$  group is well displayed at  $704 \text{ cm}^{-1}$ , which is not exhibited in the spectrum of  $\text{CO}_3$ -bearing apatite with  $\sim 3 \text{ wt}\%$   $\text{CO}_2$ .

### Stracherite structure

The crystal structure of stracherite was refined from diffraction data collected from a fragment of the crystal shown in Figure 2a. The composition of the same grain was also investigated (Table 1). Experimental data and the results of the structure refinement are given in the supplementary information (Supplemental<sup>1</sup> Tables S1–S3) and can also be found within the CIF<sup>1</sup>.

Stracherite belongs to the zadovite group with the general crystal chemical formula  $AB_6(\text{TO}_4)_2[(\text{TO}_4)_{2-x}(\text{CO}_3)_x]W$  and  $x \approx 0$  (zadovite, aradite, and gazevite) and  $\sim 1$  (stracherite) (Galuskin et al. 2015a, 2017; Galuskina et al. 2018). The ideal modular structure type of zadovite is formed by intercalating antiperovskite layers  $\{[\text{WB}_6](\text{TO}_4)_2\}^{\text{e}+}$  with  $A(\text{TO}_4)_8$  layers (Fig. 5).

The single antiperovskite layer shows F1Ca6 anion-centered coordination polyhedra. Using a cation-centered approach, F1 is sandwiched between two layers of sevenfold Ca coordination polyhedra. The Ca polyhedra form face-sharing triplets with the common edge F1-O1. The atom F1 connects two of these triplets (one of each layer), which are related by a threefold roto inversion  $(\bar{3})$  (Fig. 6).

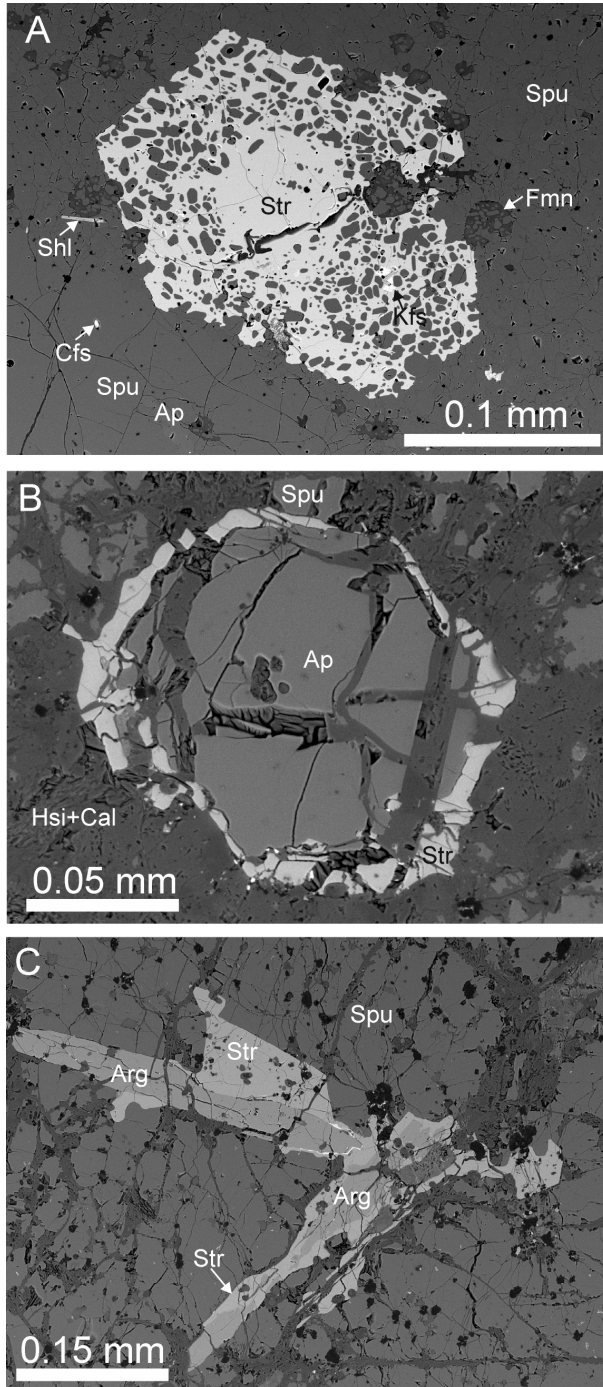


**FIGURE 3.** (a) Stracherite metacrysts in spurrite rock, associated with large spurrite crystals at the left bottom corner in the image, cross section of stracherite sub-perpendicular to *c*. (b) Partial substitution of stracherite for CO<sub>3</sub>-bearing fluorapatite. (c) Stracherite grows on ariegilite and partially substitutes for it. Ap = fluorapatite; Arg = ariegilite; Cal = calcite; Cfs = undiagnosed Ca-Fe sulfide; Kfs = undiagnosed K-Fe sulfide in composition close to KFeS<sub>2</sub>; Fmn = fluormayenite-fluorkyuygenite, Hsi = undiagnosed hydrosilicates, Shl = shulamite, Spu = spurrite, Str = stracherite.

**TABLE 1.** Chemical composition of stracherite and associated CO<sub>3</sub>-bearing fluorapatite, wt%

	Stracherite			Fluorapatite mean 2
	Mean 22	S.D.	Range	
SO <sub>3</sub>	1.94	0.09	1.79–2.10	n.d.
P <sub>2</sub> O <sub>5</sub>	11.24	0.25	10.71–11.69	33.78
V <sub>2</sub> O <sub>5</sub>	0.18	0.07	0–0.31	n.d.
SiO <sub>2</sub>	15.11	0.12	14.92–15.36	3.73
TiO <sub>2</sub>	0.09	0.02	0.05–0.13	n.d.
Al <sub>2</sub> O <sub>3</sub>	0.09	0.02	0.04–0.12	0.16
CaO	45.49	0.14	45.22–45.73	56.44
BaO	19.85	0.23	19.19–20.20	n.d.
SrO	n.d.			0.20
Na <sub>2</sub> O	0.05	0.02	0.03–0.11	0.08
K <sub>2</sub> O	0.11	0.01	0.09–0.14	0.17
F	2.44	0.10	2.20–2.63	3.23
CO <sub>2</sub> *	4.44			2.97
H <sub>2</sub> O*				0.23
–O=F	1.03			1.36
	100.00			99.63
Ba	0.96 <sup>a</sup>			0.01 <sup>b</sup>
Sr				0.02
K	0.02			0.01
Na	0.01			0.01
Ca	6.01			4.96
A(+B)	7.00			5.00
SiO <sub>4</sub> <sup>4-</sup>	1.86			0.31
TiO <sub>4</sub> <sup>4-</sup>	0.01			
AlO <sub>4</sub> <sup>5-</sup>	0.01			0.01
PO <sub>4</sub> <sup>3-</sup>	1.17			2.35
SO <sub>4</sub> <sup>2-</sup>	0.18			
VO <sub>3</sub> <sup>3-</sup>	0.02			
CO <sub>3</sub> <sup>2-</sup>	0.75			0.33
T	4.00			3.00
F <sup>-</sup>	0.95			0.84
O <sup>2-</sup>	0.03			
OH				0.13
W	0.98			0.97

Notes: \* calculated on charge balance; n.d. = not detected.

<sup>a</sup> Normalized on 7 (Ba+K+Na+Ca).

<sup>b</sup> Normalized on 5 (Ca+Sr+K+Na).

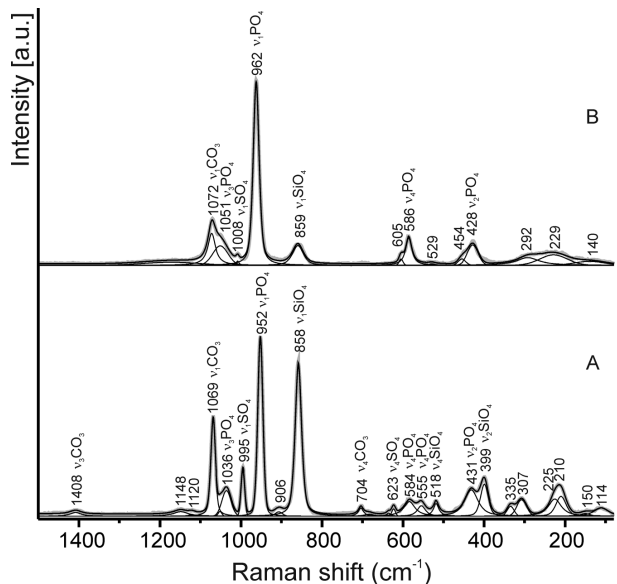


**FIGURE 4.** Raman spectra of stracherite (a) and CO<sub>3</sub>-bearing fluorapatite (b) with fitted bands.

The same kind of the layers composed of (Ca,Na)-triplets,  $[(Ca,Na)_3O_{11-14}]$ , with octahedral structural cages occupied by anions, were described earlier for several minerals exhibiting elements of hexagonal antiperovskite structure (Sokolova et al. 1999, 2005; Sokolova and Hawthorne 2001; Krivovichev 2008).

In stracherite, antiperovskite modules  $[FCa_6(SiO_4)_2]^{3+}$  intercalate with  $[Ba(PO_4)(CO_3)]^{3-}$  layers. In addition to atom positions of the zadovite structure, the position of C atoms in stracherite was located from difference Fourier maps, 0.3 Å from the center of the  $T2O_4$  tetrahedra and the threefold axis (Figs. 7a and 7b). Therefore,  $(CO_3)^{2-}$  triangles are statistically distributed over three equivalent positions, parallel to three faces of the tetrahedra (Fig. 7b). In the  $T2O_4$  tetrahedra, the T2-atom has one bond to the apical oxygen O4 and three bonds to the O3 atoms in the base. In the planar  $(CO_3)^{2-}$  group, carbon is bonded to O4 and to two of the three O3 atoms at the base of the substituted tetrahedra (Fig. 7b). Therefore, substitution of a  $(PO_4)^{3-}$  tetrahedron by a  $(CO_3)^{2-}$  group, results in formation of vacancies at the O3 sites (Fig. 7b), which is evident from the refinement results (reduced site occupancy of O3, Supplemental<sup>1</sup> Table S2). The O4 position does not show any reduced occupancy, which excludes the location of the  $(CO_3)^{2-}$  group at the base of the replaced tetrahedra.

The 40% substitution of  $CO_3$  groups for  $PO_4$  tetrahedra results in cation and anion disorder. The occupancy of the O3 site decreases from 100 to 87% and hence the Ba atom is coordinated by 5.22 oxygen atoms (instead of 6) on the O3 site. To compensate for the decrease in bond-valence contribution from anions at the O3 site, the O2 site splits into two subsites: O2 and

O2A (Figs. 7a and 7c). The bond-lengths Ba-O2 and Ba-O2A are 3.444(7) and 3.032(8) Å (Table 2). The shorter bond-length Ba-O2A increases the bond-valence sum of the Ba atom by 0.08 valence units (v.u.) (Table 2). That exactly compensates the decreased contribution from O atoms on the O3 site (Table 2). In fact, the site occupancy of the O2A site corresponds to the occupancy of the C site.

This kind of occupational and positional disorder in  $T2O_4/CO_3$  is responsible for the unusual bond distances observed in the tetrahedra [ $T2-O3 = 1.472(3)$  Å and  $T2-O4 = 1.500(4)$  Å], as well as in the  $(CO_3)^{2-}$  group [ $C1-O3 = 1.37(5)$  and  $C1-O4 =$

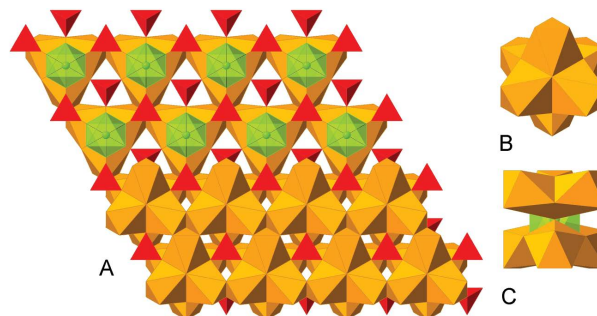


**FIGURE 6.** (a) Ideal antiperovskite module in the zadovite-type structure is composed of two layers formed by Ca-triplets  $Ca_3O_{14}$  (yellow), with Si-tetrahedra (red) located in the gaps. (b) Triplets are rotated relative to each other by  $60^\circ$ . (c) The octahedral sites between the triplets are occupied by F/O (green octahedra).

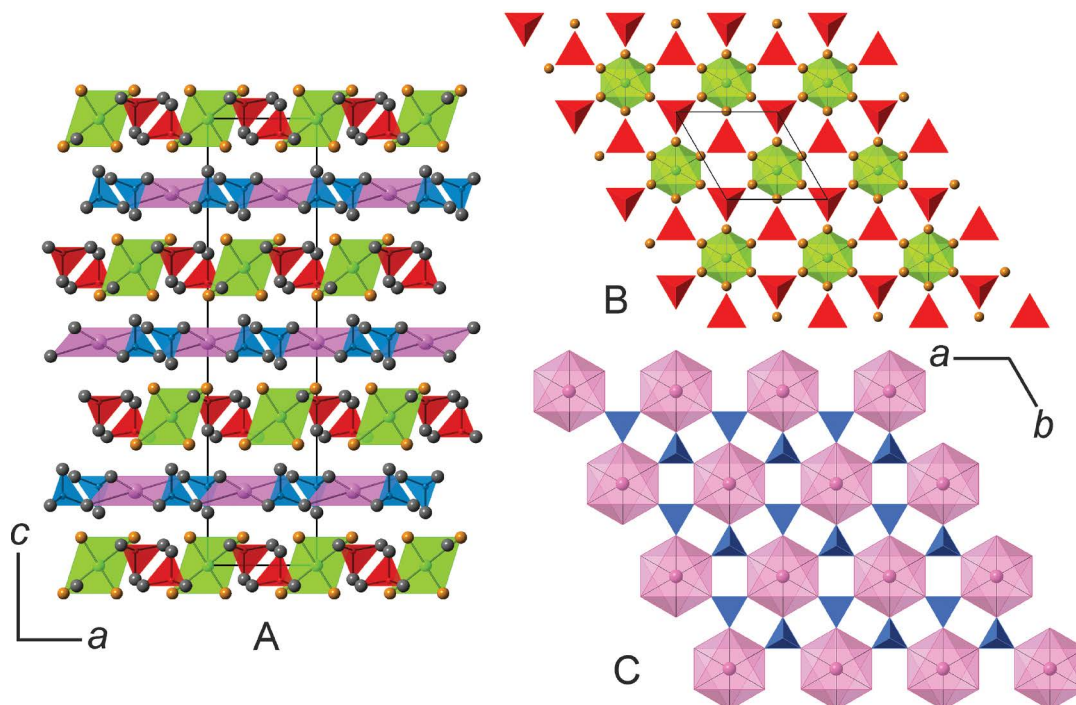


**FIGURE 5.** (a) Ideal structure of stracherite,  $BaCa_6(SiO_4)_2[(PO_4)(CO_3)]F$ , is easiest described as a 1:1 stacking of the two modules (b)  $[(FCa_6)(SiO_4)_2]^{3+}$  and (c)  $[Ba(PO_4)(CO_3)]^{3-}$  along [001] ( $CO_3$  groups are not shown). Module b consists of F1 octahedra (green) that are coordinated by 6 Ca atoms (yellow spheres) with  $(SiO_4)$  tetrahedra filling the gaps (red T1 tetrahedra). Module c is characterized by  $PO_4$ -tetrahedra (blue) connected to sixfold-coordinated Ba (purple translucent octahedra).

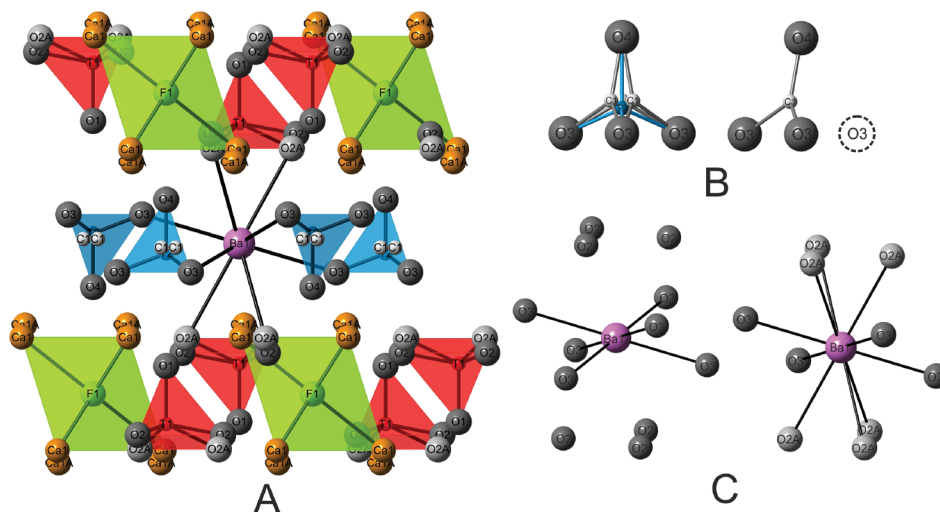


**FIGURE 7.** (a) A fragment of the stracherite structure,  $\text{BaCa}_6(\text{SiO}_4)_2[(\text{PO}_4)(\text{CO}_3)]\text{F}$ , showing the split Ca1 and O2 sites and also the T2/C1 sites. (b)  $\text{CO}_3$  groups, which replace  $\sim 40\%$  with  $\text{PO}_4$  tetrahedra, take positions on three faces of the tetrahedra always including the apical O4 atom (on the left). Carbon occupies one of three symmetric sites centering the O3-O3-O4 triangle, with the opposite O3 site vacant (dashed, on the right). (c) Oxygen sites surrounding the Ba site: sixfold coordination of Ba in C free domains (on the left); 10-fold coordination of Ba in the case of appearing of two vacancies at O3 sites (on the right) in C-bearing domains. Color coding as in Figure 5. O2, O2A, and O3 (light gray) are oxygen sites with the incomplete occupation.

1.44(2) Å, Table 2]. These distances represent values somewhat intermediate between the expected tetrahedral P-O ( $\sim 1.53$  Å) and planar C-O ( $\sim 1.28$  Å) distances (Shannon 1976). This can be observed in the O-O distances too. In a typical planar  $(\text{CO}_3)^{2-}$  group (calcite, aragonite) the triangular O-O distance is 2.23 Å (Graf 1961), whereas in a  $(\text{PO}_4)^{3-}$  tetrahedron the O-O distance is 2.50 Å (Hughes et al. 1989). In stracherite the O3-O3 distance is 2.38 Å and thus intermediate between  $(\text{CO}_3)^{2-}$  and  $(\text{PO}_4)^{3-}$ . Disordered substitution of about 40% of the  $(\text{PO}_4)^{3-}$ -tetrahedra by planar  $(\text{CO}_3)^{2-}$  groups causes a significant deviation of the stracherite structure from the “ideal” zadovite structure.

## DISCUSSION

Stracherite,  $\text{BaCa}_6(\text{SiO}_4)_2[(\text{PO}_4)(\text{CO}_3)]_2\text{F}$ , is the first intercalated hexagonal antiperovskite containing carbonate groups.  $(\text{CO}_3)^{2-}$  groups substitute for  $(\text{PO}_4)^{3-}$  according to the mechanism known in  $\text{CO}_3$ -bearing apatite of the B-type, where  $(\text{CO}_3)^{2-}$  group is randomly located sub-parallel to one of the faces of a  $(\text{PO}_4)^{3-}$  tetrahedron (Borneman-Starinkevich and Belov 1953; Ivanova et al. 2001; Fleet and Liu 2004). In stracherite, about 40% of  $(\text{PO}_4)^{3-}$  tetrahedra are substituted by  $(\text{CO}_3)^{2-}$  groups. Theoretically, substitution of  $(\text{PO}_4)^{3-}$  by  $(\text{CO}_3)^{2-}$  causes the appearance of two vacancies among six sites of O3 coordinating Ba1 and the shift of six O2 O atoms (two O2-O2-O2 triangles) to O2A positions (Figs. 7a and 7c). Occupation of ca. 0.87 for O3 (Supplemental<sup>1</sup> Table S2) gives 5.22 atoms on six O3 sites. Therefore, 0.78 sites of six O3 are not occupied, half of this ( $0.78/2 = 0.39$ ) corresponds to vacancies at T2 (occupation 0.396) and occupation of C1 is  $3 \times 0.132 = 0.396$  and O2A = 0.443 (Supplemental<sup>1</sup> Table S2).

The substitution of  $(\text{CO}_3)^{2-}$  for  $(\text{PO}_4)^{3-}$  groups affects the coordination of the O4 atom. The O4 atom exhibits a bond valence sum (BVS) of 2.27 when it is coordinated by T2 and three Ca1

(Table 2). This coordination is changed to one carbon and three Ca-atoms when a  $(\text{CO}_3)^{2-}$  group is present. A part of the Ca-atoms (19%) is shifted from Ca1 to the Ca1A site (Fig. 7a). Therefore, O4 is either coordinated by one Ca1A and two Ca1 (BVS 2.25) or by one C and three Ca1 resulting in a BVS of 1.95 (Table 2).

The sum formula resulting from the final structure refinement is  $\text{BaCa}_6[(\text{SiO}_4)_{1.79}(\text{PO}_4)_{0.21}][(\text{PO}_4)_{1.21}(\text{CO}_3)_{0.79}]\Sigma_{22}\text{F}$ , however, the formula is not charge neutral ( $-0.21$  electrons). In stracherite, besides Si, a slight amount of phosphorus is located on site T1, and besides P, S enters in T2. There are two alternative ways to obtain a charge-balanced formula, depending on whether sulfur is present or not:  $\text{BaCa}_6[(\text{SiO}_4)_{1.79}(\text{PO}_4)_{0.21}][(\text{PO}_4)_{1.21}(\text{CO}_3)_{0.79}]\Sigma_{22}\text{F}$  and  $\text{BaCa}_6(\text{SiO}_4)_2[(\text{PO}_4)_{1.00}(\text{SO}_4)_{0.21}(\text{CO}_3)_{0.79}]\Sigma_{22}\text{F}$ . Both variants lead to the idealized formula of the stracherite end-member  $\text{BaCa}_6(\text{SiO}_4)_2[(\text{PO}_4)(\text{CO}_3)]\text{F}$ .

To obtain a charge-balanced empirical formula from the electron microprobe results, a slightly lower  $(\text{CO}_3)^{2-}$  content is needed in comparison to the structure refinement:  $(\text{Ba}_{0.96}\text{K}_{0.02}\text{Na}_{0.01})\Sigma_{0.99}\text{Ca}_{6.01}[(\text{SiO}_4)_{1.86}(\text{PO}_4)_{0.12}(\text{AlO}_4)_{0.01}(\text{TiO}_4)_{0.01}]\Sigma_{22}[(\text{PO}_4)_{1.05}(\text{SO}_4)_{0.18}(\text{CO}_3)_{0.75}(\text{VO}_4)_{0.02}]\Sigma_{22}(\text{F}_{0.95}\text{O}_{0.03})\Sigma_{0.98}$ .

Stracherite is a relatively stable mineral. Our observations show that it does not alter in low-temperature processes, whereas associated spurrite is completely substituted by secondary hydrosilicates and calcite. The formation of large arriegilite and stracherite crystals (up to 0.5 mm) is related to high-temperature alterations of primary spurrite marbles under the influences of by-products (gases, fluids) of combustion metamorphism generated in different burning foci. Gases penetrate into earlier formed high-temperature rocks through cracks or linear channels (microfumaroles; Fig. 1), that lead to re-crystallization of primary clinker minerals. The re-crystallization products include large spurrite and calcite metacrystals (up to 1 cm) and phosphorus-bearing layered antiperovskites. The largest stracherite crystals

**TABLE 2.** Selected interatomic distances (Å) and calculated bond valence sum (BVS; Brown and Altermatt 1985) for stracherite

Atom-atom	Distance	Atom-atom	Distance
Ba1 <sup>a</sup> -O3	2.835(2) × 6	O1 <sup>b</sup> -Ca1A	2.471(9) × 3
-O2	3.444(7) × 6	-T1	1.623(3)
BVS	1.67(1)	BVS	2.41(2)
Ba1 <sup>b</sup> -O3	2.835(2) × 4	O2 <sup>b</sup> -Ba1	3.444(7)
-O2A	3.032(8) × 6	-Ca1	2.330(5) × 2
BVS	1.75(2)	-Ca1	2.770(8)
Ca1-O1	2.244(3)	-T1	1.620(5)
-O2	2.330(5) × 2	BVS	1.97(2)
-O4	2.438(3)	O2 <sup>b</sup> -Ba1	3.444(7)
-F1	2.543(2)	-Ca1A	2.395(7) × 2
-O3	2.589(3) × 2	-T1	1.621(7)
-O2	2.770(8)	BVS	1.73(2)
BVS	2.20(2)	O3 <sup>b</sup> -Ba1	2.835(2)
Ca1A-O4	2.175(10)	-Ca1	2.589(3) × 2
-O2A	2.380(8) × 2	-T2	1.472(2)
-O3	2.409(7) × 2	BVS	2.13(1)
-O1	2.471(9)	O3 <sup>b</sup> -Ba1	2.834(2)
-F1	2.713(8)	-Ca1A	2.409(7) × 2
BVS	2.25(2)	-C1	1.44(2)
T1 <sup>a</sup> -O2	1.621(7) × 3	BVS	1.73(1)
-O1	1.623(3)	O4 <sup>a</sup> -Ca1	2.438(3) × 3
BVS	4.15(2)	-T2	1.500(4)
T1 <sup>b</sup> -O2A	1.628(10) × 3	BVS	2.27(2)
-O1	1.623(3)	O4 <sup>b</sup> -Ca1	2.438(3) × 3
BVS	4.07(3)	-C1	1.37(4)
T2-O3	1.472(2) × 3	BVS	1.95(2)
-O4	1.500(4)	O4 <sup>c</sup> -Ca1A	2.175(10)
BVS	5.97(2)	-Ca1	2.438(3) × 2
C1-O3	1.44(2) × 2	-C1	1.37(4)
-O4	1.37(4)	BVS	2.25(2)
BVS	2.92(1)	F1 <sup>a</sup> -Ca1	2.543(2) × 6
O1 <sup>a</sup> -Ca1	2.244(3) × 3	BVS	0.93(1)
-T1	1.623(3)	F1 <sup>b</sup> -Ca1	2.542(3)
BVS	2.49(1)	-Ca1A	2.713(8) × 5
		BVS	0.65(2)

Notes: <sup>abc</sup> Alternate coordination environments.

were found in walls of “fumaroles” in association with compositionally exotic sulfides. Gaseous phases were also involved in their formation (Figs. 2 and 3a). Until now, stracherite was only found in recrystallized spurrite marbles at one single outcrop at the Hatrurim Basin, Negev Desert.

### GENETIC IMPLICATION

In pyrometamorphic rocks of the Hatrurim Complex, intercalated hexagonal antiperovskites are presented by minerals of the zadovite and the nabimusaite group. Minerals of both groups differ in origin. Zadovite, BaCa<sub>6</sub>[(SiO<sub>4</sub>)(PO<sub>4</sub>)](PO<sub>4</sub>)<sub>2</sub>F, and aradite, BaCa<sub>6</sub>[(SiO<sub>4</sub>)(VO<sub>4</sub>)](VO<sub>4</sub>)<sub>2</sub>F, form a solid solution and crystallize in paralavas confined to gehlenite-larnite (flamite) hornfelses (Galuskin et al. 2015b). Gazeevite, BaCa<sub>6</sub>(SiO<sub>4</sub>)<sub>2</sub>(SO<sub>4</sub>)<sub>2</sub>O, and minerals of the nabimusaite group: nabimusaite, KCa<sub>12</sub>(SiO<sub>4</sub>)<sub>4</sub>(SO<sub>4</sub>)<sub>2</sub>O<sub>2</sub>F, dargaite, BaCa<sub>12</sub>(SiO<sub>4</sub>)<sub>4</sub>(SO<sub>4</sub>)<sub>2</sub>O<sub>3</sub>, and ariegilatite, BaCa<sub>12</sub>(SiO<sub>4</sub>)<sub>4</sub>(PO<sub>4</sub>)<sub>2</sub>OF<sub>2</sub>, form in larnite marbles. Their genesis is a result of reactions of minerals of early clinker association, such as fluorellestadite-fluorapatite, larnite, and oldhamite, with by-products of pyrometamorphism (Galuskin et al. 2015b, 2017, 2018; Galuskina et al. 2018). Ariegilatite is the only phase that was found in larnite as well as in spurrite rocks. All intercalated hexagonal antiperovskites are found in numerous outcrops of pyrometamorphic rocks in the territories of Israel, Palestine, and Jordan (Galuskin et al. 2015a, 2015b; 2017, 2018; Galuskina et al. 2018). Stracherite, BaCa<sub>6</sub>(SiO<sub>4</sub>)<sub>2</sub>[(PO<sub>4</sub>)(CO<sub>3</sub>)]F, is an exception because it

was found in spurrite marble in association with ariegilatite at the single outcrop in the Hatrurim Basin, Negev Desert, Israel. As discussed, the formation of stracherite and ariegilatite is related to reactions of by-products of combustion metamorphism with early minerals of clinker association, mainly with CO<sub>3</sub>-bearing fluorapatite. The genesis of all intercalated hexagonal antiperovskites is not connected with the main pyrometamorphic event of the Hatrurim Complex rock formation. The main stage of rock genesis resulted in very high-temperature water-free mineral association resembling natural ceramics and close in mineral content to cement clinkers forming after sedimentary protolith. The pyrometamorphic process, during which rocks of the Hatrurim Complex were formed, was relatively extended with numerous burning foci, which generated different by-products such as melts, fluids, and gases. Heterogeneous sedimentary protolith defines formation of not only main types of pyrometamorphic rocks (spurrite and larnite marbles, gehlenite hornfelses), but also determines the character of succeeding alterations. Just so, paralavas with minerals of the zadovite-aradite series crystallized from partial melts generated at gehlenite hornfels unit (Galuskin et al. 2015a). In larnite-bearing marble primary fluorellestadite was substituted by (SO<sub>4</sub>)<sup>2-</sup>-bearing hexagonal antiperovskites: nabimusaite, dargaite, and gazeevite (Galuskin et al. 2015b, 2017; Galuskina et al. 2018). In spurrite-bearing marble, CO<sub>3</sub>-bearing apatite was a precursor for (PO<sub>4</sub>)<sup>3-</sup>-bearing antiperovskite formation: ariegilatite and stracherite (Fig. 3c). That way, pyrometamorphic reactions of by-products with early-formed minerals induced an increasing diversity of high-temperature minerals in the Hatrurim Complex.

### ACKNOWLEDGMENTS

The authors thank Elena Sokolova and Fernando Camara for their careful review that improved the manuscript. The investigations were partially supported by the National Science Centre (NCN) of Poland, grant no. 2016/23/B/ST10/00869. The authors are grateful to Thomas Armbruster for helpful discussion.

### REFERENCES CITED

- Banno, Y., Miyawaki, R., Momma, K., and Bunno, M. (2016) CO<sub>3</sub>-bearing member of the hydroxylapatite-hydroxyllellestadite series from Tadano, Fukushima Prefecture, Japan: CO<sub>3</sub>-SO<sub>4</sub> substitution in the apatite-ellestadite series. *Mineralogical Magazine*, 80, 363–370.
- Borneman-Starinkevich, I.D., and Belov, N.V. (1953) Carbonate-apatites. *Doklady Akademii Nauk SSSR*, 90, 89–92.
- Brown, I.D., and Altermatt, D. (1985) Bond-valence parameters obtained from a systematic analysis of the inorganic crystal structure database. *Acta Crystallographica*, B41, 244–247.
- Comodi, P., and Liu, Y. (2000) CO<sub>3</sub> substitution in apatite: further insight from new crystal-chemical data of Kasekere (Uganda) apatite. *European Journal of Mineralogy*, 12, 965–974.
- Fleet, M.E., and Liu, X. (2004) Location of type B carbonate ion in type A–B carbonate apatite synthesized at high pressure. *Journal of Solid State Chemistry*, 177, 3174–3182.
- Galuskin, E.V., Gfeller, F., Galuskina, I.O., Pakhomova, A., Armbruster, T., Vapnik, Y., Włodyka, R., Dzierzanowski, P., and Murashko, M. (2015a) New minerals with modular structure derived from hatrurite from the pyrometamorphic Hatrurim Complex, Part II: Zadovite, BaCa<sub>6</sub>[(SiO<sub>4</sub>)(PO<sub>4</sub>)](PO<sub>4</sub>)<sub>2</sub>F, and aradite, BaCa<sub>6</sub>[(SiO<sub>4</sub>)(VO<sub>4</sub>)](VO<sub>4</sub>)<sub>2</sub>F, from paralavas of the Hatrurim Basin, Negev Desert, Israel. *Mineralogical Magazine*, 79, 1073–1087.
- Galuskin, E.V., Gfeller, F., Armbruster, T., Galuskina, I.O., Vapnik, Ye., Murashko, M., Włodyka, R., and Dzierzanowski, P. (2015b) New minerals with modular structure derived from hatrurite from the pyrometamorphic Hatrurim Complex, Part I: Nabimusaite, KCa<sub>12</sub>(SiO<sub>4</sub>)<sub>4</sub>(SO<sub>4</sub>)<sub>2</sub>O<sub>2</sub>F, from larnite rock of the Jabel Harmun, Palestinian Autonomy, Israel. *Mineralogical Magazine*, 79, 1061–1072.
- Galuskin, E.V., Gfeller, F., Galuskina, I.O., Armbruster, T., Krztałta, A., Vapnik Ye., Kusz, J., Dulski, M., Gardocki, M., Gurbanov, A.G., and Dzierzanowski, P. (2017) New minerals with a modular structure derived from hatrurite from the pyrometamorphic rocks. Part III. Gazeevite, BaCa<sub>6</sub>(SiO<sub>4</sub>)<sub>2</sub>(SO<sub>4</sub>)<sub>2</sub>O, from

- Israel and the Palestine Autonomy, South Levant, and from South Ossetia, Greater Caucasus. *Mineralogical Magazine*, 81, 499–513.
- Galuskin, E.V., Krüger, B., Galuskina, I.O., Krüger, H., Vapnik, Y., Wojdyla, J.A., and Murashko, M. (2018) New mineral with modular structure derived from hatrurite from the pyrometamorphic rocks of the Hatrurim Complex: ariegilatite,  $\text{BaCa}_{12}(\text{SiO}_4)_6(\text{PO}_4)_2\text{F}_2\text{O}_3$ , from Negev Desert, Israel. *Minerals*, 8, 109.
- Galuskina, I.O., Gfeller, F., Galuskin, E.V., Armbruster, T., Vapnik, Ye., Dulski, M., Gardocki, M., Jezak, L., and Murashko, M. (2018) New minerals with modular structure derived from hatrurite from the pyrometamorphic rocks, part IV: Dargaite,  $\text{BaCa}_{12}(\text{SiO}_4)_4(\text{SO}_4)_2\text{O}_3$ , from Nahal Darga, Palestinian Autonomy. *Mineralogical Magazine*, 82. <https://doi.org/10.1180/minmag.2017.081.095>
- Graf, D.L. (1961) Crystallographic tables for the rhombohedral carbonates. *American Mineralogist*, 46, 1283–1316.
- Hughes, J.M., Cameron, M., and Crowley, K.D. (1989) Structural variations in natural F, OH, and Cl apatites. *American Mineralogist*, 74, 870–876.
- Ivanova, T.I., Frank-Kamenetskaya, O.V., Kol'tsov, A.B., and Ugolkov, V.L. (2001) Crystal structure of calcium-deficient carbonated hydroxyapatite. Thermal decomposition. *Journal of Solid State Chemistry*, 160, 340–349.
- Jeffery, J.W. (1952) The crystal structure of tricalcium silicate. *Acta Crystallographica*, 5, 26–35.
- Kabsch, W. (2010) XDS. *Acta Crystallographica*, D166, 125–132.
- Krivovichev, S.V. (2008) Minerals with antiperovskite structure: a review. *Zeitschrift für Kristallographie*, 223, 109–113.
- Krüger, B., Galuskin, E.V., Galuskina, I.O., Krüger, H., Vapnik, Y., Wojdyla, J.A., and Murashko, M. (2017a) Ariegilatite, a new mineral with modular structure. *Mitteilungen der Österreichischen Mineralogischen Gesellschaft*, 163, 58.
- Krüger, B., Galuskin, E.V., Galuskina, I.O., Krüger, H., Vapnik, Y., Olieric, V., and Pauluhn, A. (2017b) A potentially new mineral with a modular structure based on antiperovskite layers. *Mitteilungen der Österreichischen Mineralogischen Gesellschaft*, 163, 59.
- Mandarino, J.A. (2007) The Gladstone-Dale compatibility of minerals and its use in selecting mineral species for further study. *Canadian Mineralogist*, 45, 1307–1324.
- Penel, G., Leroy, G., Rey, C., and Bres, E. (1998) MicroRaman spectral study of the  $\text{PO}_4$  and  $\text{CO}_3$  vibrational modes in synthetic and biological apatites. *Calcified Tissue International*, 63, 475–481.
- Shannon, R.D. (1976) Revised effective ionic radii and systematic studies of interatomic distances in halides and chalcogenides. *Acta Crystallographica*, A32, 751–767.
- Sheldrick, G.M. (2008) A short history of SHELX. *Acta Crystallographica*, A64, 112–122.
- Sokolova, E., and Hawthorne, F.C. (2001) The crystal chemistry of the  $[\text{M}_3\text{O}_{11-14}]$  trimeric structures: from hypergpaite complexes to saline lakes. *Canadian Mineralogist*, 39, 1275–1294.
- Sokolova, E.V., Yamnova, N.A., Egorov-Tismenko, Yu.K., and Khomyakov, A.P. (1984) Crystal structure of arctite, a new sodium calcium barium phosphate  $(\text{Na}_2\text{Ca})\text{Ca}_6\text{Ba}[\text{PO}_4]_6\text{F}_3$ . *Soviet Physics Doklady*, 29, 5–8.
- Sokolova, E.V., Kabalov, Yu.K., Ferraris, G., Schneider, J., and Khomyakov, A.P. (1999) Modular approach in solving the crystals structure of a synthetic dimorph of nacaphite  $\text{Na}_2\text{Ca}[\text{PO}_4]\text{F}$ , from powder-diffraction data. *Canadian Mineralogist*, 37, 83–90.
- Sokolova, E., Hawthorne, F.C., and Khomyakov, A.P. (2005) Polyphite and sobolevite: revision of their crystal structures. *Canadian Mineralogist*, 43, 1527–1544.
- Vapnik, Y., Sharygin, V.V., Sokol, E.V., and Shagam, R. (2007) Paralavas in a combustion metamorphic complex: Hatrurim Basin, Israel. *Reviews in Engineering Geology*, 18, 1–21.
- Vapnik, Y., Galuskina, I., Palchik, V., Sokol, E.V., Galuskin, E., Lindsley-Griffin, N., and Stracher, G.B. (2015) Stone-tool workshops of the Hatrurim Basin, Israel: mineralogy, geochemistry, and rock mechanics of lithic industrial materials. In G.B. Stracher, A. Prakash, and E.V. Sokol, Eds., *Coal and Peat Fires: A Global Perspective*, 3, p. 281–316. Elsevier.
- Waltersperger, S., Olieric, V., Pradervand, C., Gletting, W., Salathe, M., Fuchs, M.R., Curtin, A., Wang, X., Ebner, S., Panepucci, E., Weinert, T., Schulze-Briese, C., and Wang, M. (2015) PRIGO: a new multi-axis goniometer for macromolecular crystallography. *Journal of Synchrotron Radiation*, 22(4), 895–900.

MANUSCRIPT RECEIVED FEBRUARY 2, 2018

MANUSCRIPT ACCEPTED JUNE 1, 2018

MANUSCRIPT HANDLED BY FABRIZIO NESTOLA

#### Endnote:

<sup>1</sup>Deposit item AM-18-106493, Supplemental Tables. Deposit items are free to all readers and found on the MSA web site, via the specific issue's Table of Contents (go to [http://www.minsocam.org/MSA/AmMin/TOC/2018/Oct2018\\_data/Oct2018\\_data.html](http://www.minsocam.org/MSA/AmMin/TOC/2018/Oct2018_data/Oct2018_data.html)).